Dalton Transactions

Accepted Manuscript

ROYAL SOCIETY OF CHEMISTRY

www.rsc.org/dalton

Cite this: DOI: 10.1039/c0xx00000x

www.rsc.org/xxxxxx

ARTICLE TYPE

Antitumor Properties of Platinum(IV) Prodrug-Loaded Silk Fibroin Nanoparticles

A. Abel Lozano-Pérez,[a] Ana L. Gil,[b] Sergio A. Pérez,[b] Natalia Cutillas,[b] Hajo Meyer,[c] Mónica Pedreño,[b] Salvador Aznar-Cervantes,[a] Christoph Janiak,[c] Jose Luis Cenis,[a] and José Ruiz*[b]

Received (in XXX, XXX) Xth XXXXXXXXX 20XX, Accepted Xth XXXXXXXXX 20XX

DOI: 10.1039/b000000x

Platinum(IV) complexes take advantage of the exclusive conditions that occur within the tumor to carry out their cytotoxic activity. On the other hand, silk fibroin has natural properties which make it very interesting as a biomaterial: highly biocompatible, biodegradable, low immunogenicity, high cellular penetration capacity and high reactive surface. Herein we report the preparation of silk fibroin nanoparticles (SFNs) loaded with the hydrophobic Pt(IV) complex *cis,cis,trans*-[$Pt(NH_3)_2Cl_2(O_2CC_6H_5)_2$] (PtBz). Only a small fraction of the loaded PtBz is released (less than 10% after 48 h). PtBz-SFNs trigger strong cytotoxic effects against human ovarian carcinoma A2780 cells and its cisplatin-resistant variant A2780cisR cells. Interestingly, PtBz-SFNs are very cytotoxic (nanomolar IC_{50} values) toward the triple negative breast tumor cell line MDA-MB-231, and also toward SK-BR-3 and MCF-7, while maintaining an excellent selectivity index.

1. Introduction

Platinum(II) drugs are effective anticancer agents against many malignancies including testicular, ovarian, bladder, and non small-cell lung cancer.[1] In clinics, cisplatin (CDDP) is one of the most widely used anticancer drugs, which can bind to genomic DNA. However, like most of the other small-molecule anticancer drugs, its clinical use is limited by high toxicity and severe side-effects,[2,3] usually nephrotoxicity and neurotoxicity, as well as incidences of Pt associated drug resistance.[4] Surrounded by six ligands in an octahedral coordination environment, the hydrophobic platinum(IV) metal centre PtBz (Figure 1) is more inert towards substitution reactions than platinum(II). Upon reduction in the tumor cells by several intracellular reducing agents such as glutathione, metallothionein, cysteine, and ascorbic acid, two axial ligands are released and the hydrophilic divalent CDDP species is generated.[5,6]

Nanoparticles have drawn particular attention in recent years because they can facilitate the delivery of therapeutic drugs taking advantage of nanosized porous tumor vasculatures coupled with poor lymphatic clearance and slow venous return in these tissues, *i.e.*, the enhanced permeability and retention (EPR) effect.[7–14] Nanocarrier-based delivery of platinum compounds is one such area of intense research effort and may allow the development of the next generation of platinum chemotherapy.[15–26]

On the other hand, natural polymers such as proteins and polysaccharides represent a very promising biomedical platform because of their renewability, nontoxicity, biocompatibility, and biodegradability.[27–32] One such polymeric nanoparticle is silk fibroin protein,[33–35] which shows low immunogenicity.[36]

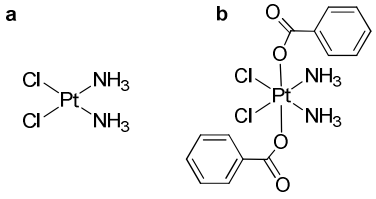

Fig. 1 Chemical structure of (a) cisplatin CDDP and (b) hydrophobic platinum(IV) prodrug PtBz.

Silk fibroin protein obtained from domesticated mulberry silkworm *Bombyx mori* is a protein based biomacromolecule composed of 5507 amino acid consisting of repeated sequences of six residues of $(Gly\text{-}Ala\text{-}Gly\text{-}Ala\text{-}Gly\text{-}Ser)_n$ repeats.[37] Silk fibroin has been widely used in blood vessel, skin, bone, cartilage and nervous tissue scaffolds.[38–43] SFNs loaded with some antitumor drugs such as paclitaxel [29], methotrexate,[34] doxorubicin,[36,44] and CDDP[45] (chemically combined *via* coordinate bonds) have been recently reported.

Here we disclose novel Pt(IV)-SFNs which exhibit strong cytotoxic effects in the CDDP resistant cells A2780cisR and a panel of breast cancer cell lines. These constructs have been further studied for cell cycle arrest and apoptosis. We choose an inert hydrophobic Pt(IV) analog of CDDP, PtBz (Figure 1),[46] in order to avoid CDDP deactivation by possible covalent interaction with some aminoacids of fibroin.

2. Materials and methods

Reagents, materials and apparatus

Silk fibroin was obtained from silkworms reared in the sericulture facilities of the IMIDA (Murcia, Spain). Cisplatin was provided by Alfa Aesar. PBS 1x stock solution from BDH. Purified water (18.2 MΩ·cm at 25 ºC from Millipore Direct-Q1 ultra-pure water system, Billerica, MA). MTT assay kit from Promega (Madison, USA). Solvents were dried by the usual methods. DMSO were obtained from Scharlau. All chemicals and solvents of analytical grade were used without further purification. *cis,cis,trans*-$[Pt(NH_3)_2Cl_2(OOCPh)_2]$[46] (PtBz) and SFNs[30] were prepared by procedures described elsewhere.

The platinum analyses were undertaken in an atomic absorption spectrometer (model 800, Perkin-Elmer, Shelton, USA) equipped for Zeeman-effect background correction, with a transversely heated graphite tube atomizer and AS-800 autosampler. The autosampler was not used, and the samples were pipetted manually into the atomizer. Pyrolytic graphite platforms in pyrolytically coated tubes were obtained from the same manufacturer (part number B050-4033). Argon (99.999% of purity) at 250 mL min^{-1} was used as inert gas, except during atomization, when it was stopped. Platinum hollow cathode lamp (Perkin-Elmer) was used as the radiation sources. Probes were injected at a volume of 40 µL into regular graphite wall tubes. All the measurements were done in triplicate.

Infrared spectra of synthetized complex PtBz, unloaded SFNs, and PtBz-SFNs were compared (Figure S1). Measurements were carried out on a Bruker TENSOR 37 IR spectrometer at ambient temperature in a range of 4000–500 cm^{-1}. Samples (~2 mg) were mixed with ~198 mg of KBr (Sigma-Aldrich Steinheim, Germany) grounded into a fine powder using mortar and pestle before compressing it into a disc. All the samples were analyzed in transmission mode. Nitrogen physisorption isotherms were measured on a Quantachrome Nova 4000e at 273 K. The surface area of the particles was determined from volumetric nitrogen sorption measurements at 77 K. Dynamic light scattering (DLS) and zeta potential measurements were carried out with a Malvern Zetasizer Nano Z and a Mastersizer Malvern 2000E. For the determination of the SFNs and PtBz-SFNs sizes and size distributions the dry samples were redispersed to a concentration of 1 mg/mL in 1.5 mL double deionized water via ultrasonication for 30 min. The dispersions were investigated by DLS to yield a hydrodynamic radius for SFNs in the range of 80–400 nm with an average of 110 ± 40 (standard deviation σ). The PtBz-SFNs have a broader radius distribution of 80–800 nm with an average of 120 ± 40. Transmission electron measurements were carried out on a Zeiss 902 at ambient temperature. Scanning electron measurements were carried out on a Leo 1430 VP at ambient temperature. Light microscope pictures were taken with a Carl Zeiss Axiophot 2 and a Zeiss Plan-Neofluor 63x lens with a resulting 630-times magnification. Powder X-ray diffraction (PXRD) patterns of all the samples were measured at ambient temperature on a Bruker D2 Phaser using a flat sample holder and Cu Kα radiation (λ = 1.54182 Å). Raman measurements were carried out on a Bruker MultiRam as solid sample with 900 mW laser intensity and an aperture of 6 mm. UV measurements were carried out on a Shimadzu UV-2450 UV spectrometer at ambient temperature with a concentration of 1 mg/mL. ESI mass (positive mode) analyses were performed on a HPLC/MS TOF 6220. The isotopic distribution of the heaviest set of peaks matched very closely that calculated for the formulation of the complex cation.

Preparation of Platinum(IV)-loaded nanoparticles (PtBz-SFNs), and Drug Loading Content (DLC) and Efficiency (E)

Platinum(IV)-loaded nanoparticles (PtBz-SFNs) were prepared by an incubation method. 25 mg of dried SFNs were suspended with 1 mL of platinum(IV) complex solution, from 1 to 10 mg/mL, in DMSO in Eppendorf tubes, sonicated for 4 cycles of 15 s at 30% power with pulses 15 Sec ON and 15 Sec OFF and gently agitated at 103 rpm for 72 h, protected from the light. Loaded particles were collected by centrifugation at 18000 g for 15 min. Quantity of loaded Pt(IV) prodrug was determined by an indirect method by AAS from supernatant and SFNs were washed with 500 µL MilliQ water:DMSO (15:1) and 500 µL with MilliQ water. In each phase sonicated and centrifuguged again under above condition. All batches were prepared in triplicate. PtBz-SFNs were diluted to the desired concentration immediately before use according to the equivalent dose of platinum prodrug.

Drug loading content and efficiency were presented by the equations (1) and (2), respectively:

$$\mathrm{DLC}\,(\%) = \frac{\text{weight of the drug in nanoparticles}}{\text{weight of the nanoparticles}} \times 100 \qquad (1)$$

$$\mathrm{E}\,(\%) = \frac{\text{weight of the drug in nanoparticles}}{\text{weight of the feeding drugs}} \times 100 \qquad (2)$$

Release of drug from PtBz-SFNs

The release rate of platinum complex from the silk fibroin nanoparticles in phosphate buffered saline (PBS 1x, pH 7.4) was evaluated. A suspension of PtBz-SFNs (25 mg) in water was confined (15 mL) into semipermeable Slide-A-Lyzer Dialysis cassette (3.5 KDa MWCO, Pierce-Thermo Scientific) and dialyzed against 600 mL PBS (pH 7.4) at 310 K. At a predetermined time, an aliquot of 500 µL of the external PBS was removed, and the platinum content was determined by AAS. After sampling, equal volume of fresh PBS was immediately added into the external medium.

Samples were diluted to the calibration range (10-200 µg/L) with PBS. Each assay was performed in triplicate. The amount of Pt(IV) released from the nanoparticles was expressed as a percentage of the total prodrug loaded in the nanoparticles and was plotted as a function of time.

Materials Preparation of fluorescent silk fibroin nanoparticles

Preparation of FITC (fluorescein isothiocyanate) labeled SFNs was based on the coupling reaction between the isothiocyanate group of the FITC and the primary amino group of the silk fibroin. Reaction conditions were set up following the protocol described by the supplier of the FITC. Briefly, 100 mg of FITC in 10 ml of DMSO was slowly added to 10 ml of 1 mg/mL SFNs suspension in borate buffer (50 mM, pH 8.5). The coupling reaction was allowed to proceed for 1 h at room temperature protected from the light. FITC labeled fibroin nanoparticles were then recovered using centrifugation (18000 *g* for 40 min at 4 ºC).

To remove the unconjugated FITC, the labelled SFNs were subjected to repeated cycles of washing with PBS 1x (pH 7.4) and centrifugation until no fluorescence (λ_{ex} 490 nm; λ_{em} 520 nm) was detected in the supernatant. The FITC conjugated nanoparticles were then dialyzed in a Slide-A-Lyzer Dialysis cassette (3.5 KDa MWCO, Pierce-Thermo Scientific) for 3 days in the dark against 4 L of distilled water, the water was replaced on a daily basis. Labelled SFNs were kept refrigerated and protected from light until its use.

Materials Cell Lines and Culture Conditions

Three cellular phenotypes of breast cancer were evaluated as MCF-7 (estrogen receptors), MDA-MB-231 (no estrogen receptors) or SK-BR-3 (overexpressed HER2/c-erb-2 gene) and they were grown in Dubelcco´s Modified Eagle´s Medium (DMEM) without phenol red to contain 1000 mg/L glucose suplementd with 10% (v/v) final concentration heat-inactivated Fetal Bovine Serum (FBS, Sigma, USA), 2 mM L-glutamine, 2 mM sodium pyruvate and antibiotics (penicillin/streptomicin) at 310 K in humidified atmosphere containing 7.5%-10% CO_2. Human ovarian carcinoma A2780 and A2780cis cell lines were grown in RPMI-1640, supplemented with 10% (v/v) final concentration heat-inactivated Fetal Bovine Serum (FBS, Sigma, USA), 2 mM L-glutamine and antibiotics (penicillin/streptomycin). Both cell lines were manteined at 310 K in humidified atmosphere containing 5% CO_2. In order to retain resistance to CDDP was added to A2780cisR every two subcultures at 1 μM. EA.hy926 cell line were grown in Dubelcco´s Modified Eagle´s Medium (DMEM) without phenol red to contain 1000 mg/L glucose suplementd with 10% (v/v) final concentration heat-inactivated Fetal Bovine Serum (FBS, Sigma, USA), 2 mM L-glutamine, 2 mM sodium pyruvate and antibiotics (penicillin/streptomicin) at 310 K in humidified atmosphere containing 7.5%-10% CO_2.

LLC-PK1 cell line were grown in M199 medium supplemented with 3% Fetal Bovine Serum (FBS, Sigma, USA), 2 mM L-glutamine and antibiotic (penicillin and streptomycin) at 310 K in humidified atmosphere containing 5% CO_2.

Breast cancer cell lines, EA.hy926 cell line and LLC-PK1 cell line were obtained from American Tissue Culture Collection (ATCC, U.S.A) and ovarian carcinoma cell line were obtained from European Collection of Animal Cell Culture, (ECACC, Salisbuty, U.K.).

Before and after experiments, all cell lines were micoplasma-free, as determinated by the Hoechts DNA stain method.[47] In all cases, cells from 80% confluent monolayers were removed from flasks by 0.25% trypsin solution (Sigma Aldrich.), centrifugated 200*g* 10´ and washed twice with PBS, and cell pellet diluted with complete medium. Medium was changed twice per week.

Cytotoxicity Assays

Cell proliferation was evaluated by MTT assay, (3-(4,5-dimethylthiazol-2-yl)-2,5-diphenyltetrazolium bromide. MCF-7, MDA-MB-231, SK-BR-3, A2780, A2780cis and LLC-PK1 plated in 96-well sterile plates at a density of 5×10^3 cells/well with 200 μL of medium and were then incubated for 24 h. After attachment to the culture surface, cells were incubated with various concentrations of loaded nanoparticles (PtBz-SFNs) diluted in culture medium by adding 50 μL for 72 h at 310 K. For MTT assay, the medium was removed by pipeting, then 200 μL of corresponding medium for each cell line was added and 50 μL of a MTT solution 5 mg/mL was added and left at 310 K for 4 hours at dark. Finally, this solution was removed from each plate, 100 μL of DMSO was added and shaken 5 min at 120 rpm (always at dark) before measurement. Absorbance was measured at 560 nm for MTT assays in a Fluorstar Omega spectrophotometer.

The effects of complexes were expressed as corrected percentage inhibition values according to the following equation,

$$\%\ inhibition = \left[1 - \left(\frac{T}{C}\right)\right] x\ 100$$

where T is the mean absorbance of the treated cells and C the mean absorbance in the controls.

The inhibitory potential of compounds was measured by calculating concentration-percentage inhibition curves, these curves were adjusted to the following equation:

$$E = \frac{Emax}{1 + \left(\frac{IC50}{C}\right)^n}$$

where E is the percentage inhibition observed, E_{max} is the maximal effects, IC_{50} is the concentration that inhibits 50% of maximal growth, C is the concentration of compounds tested and n is the slope of the semi-logarithmic dose–response sigmoid curves. This non-linear fitting was performed using Sigma Plot 11.0 software.

For comparison purposes, the cytotoxicity of cisplatin was evaluated under the same experimental conditions. All compounds were tested in three independent studies with quaduplicate points. The *in vitro* studies were performed in the Support Service for Experimental Sciences of the University of Murcia (Murcia, Spain).

All SFN studies and cisplatin were performed in water and in all the experiments measurements were corrected with a water control. Due to the low aqueous solubility of PtBz, it was dissolved in DMSO first and then serially diluted in complete culture medium such that the effective DMSO content was 0.4%.

TEM Sample Preparations

One million cells/well were cultured on a 6-well plate and left for 24 h at 37 ºC. Afterwards, 1 μM of the drug was added and left again for 24 h at the same temperature. The medium was then added to a Falcon™ tube. Cells were removed from the wells with trypsin and the resulting suspension put together in the Falcon™ tube with the medium. Centrifugation (200 g, 10 min) was followed, discarding the supernatant. Cells were fixed with glutaraldehyde (2.50%) for 1.5 h and then washed with washing liquid (cacodilate buffer) by means of centrifugation (same conditions). Then, addition of ethanol at increasing concentrations (30, 50, 70, 90%) for 10 min was added to the cells. Subsequently, absolute ethanol and, at the same time, copper(II) sulphate for 10 minutes were added. Then, complete dehydratation was achieved by subsequent additions of propylene

oxide in epoxy resins at higher concentrations and delays. Finally, the capsules were left in the epoxy resin for a complete night and cut to micrometer dimensions, and 70-80 nm sections were collected on mesh copper grids. The sections were imaged on a ZEIS EM10 TEM. Neither osmium tetroxide nor uranyl acetate were added during this process to ensure that contrast images were only due to the added metal drug.

Cell cycle arrest assays

Cell cycle arrest studies were performed on MCF-7, MDA-MB-231, SK-BR-3 breast cancer cells and A2780, A2780cis ovarian cancer cells. Typically, 1.5 x 10^5 cells were seeded in a 6-well plate with DMEM or RPMI medium (5 mL/plate). Cells were allowed to fix to the plate by incubation for 24 h at 310 K (7.5-10% or 5% CO_2). Then, nanoparticles (PtBz-SFNs) were added at final concentrations similar with their respective IC_{50} values in the different plates. One well for each line were untreated, for being used as a control. The cultures were incubated for other additional 24 h in the same conditions as described above. At this point, the medium was removed and stored in 15 mL Falcon™ tubes. Inmediatly, the fixed cells were treated with 1 mL of tripsine for 4 minutes at 310 K and then 1 mL of DMEM or RPMI medium containing FBS was added to stop the enzymatic action. The resulting 2 mL were added to the 15 mL Falcon™ tube. In this way both possible floating cells and adherent cells were considered for the assay. Cells were centrifugated (250 g, 10 min) and the precipitated cells were washed with 2 mL of PBS. After another centrifugation in same conditions, removed the supernadant, cells were resuspended in 200 µL of PBS. Subsequenly, 1 mL of a PBS (30%)/ethanol (70%) mix solution was aded to the cells. The solution was kept in ice for 30 minutes. The supernatant was eliminated by centrifugation (same conditions). The cells were again resuspended with 800 µL of PBS. Finally, 100 µL of RNase solution (1 mg/mL) and 100 µL of propidium iodide solution (400 µg/mL) were added. After stirring the resulting suspension was incubated at 310 K for 30 min at dark. Stainned cells were analyzed in a Becton-Dickinson FACScalibur flow cytometer. In each case 30000 events were adquired.

Apoptosis Experiments

For apoptosis determination assays, 1.5 x 10^5 cells were tipically seeded in a 6-well plate. Breast and ovarian cancer cells with compounds and their control were incubated, collected and washed twice with PBS as described above (no PBS/Etanol mix was used in this case). After removing the PBS, 40 µL of a solution containing Annexin V and PI (Annexin-V-Fluos from Roche) and 160 µL of incubation buffer (HEPES 10 mM, NaCl 140 mM, $CaCl_2$ 5 mM pH = 7.4) was added to the cell pellet. Cells were resuspended in this solution and left at room temperature in dark for 15 min. 200 µL of PBS was added immediatly previous to the measurments. These were carried out in a Beckman Coulter Epics XL flow cytometer, registering the emission at wavelengths of 620 and 525 nm for PI and Annexin V, respectively. In eache case, 10000 events were acquired.

3. Results and discussion

Preparation and characterization of PtBz-SFNs

The PtBz-SFNs were generated by suspension of lyophilized SFNs, obtained from *Bombyx mori* [31], with a PtBz [46] solution in DMSO, dispersed by sonication and then agitation for 72 h.

Fig. 2 Dynamic light scattering experiment of SFNs (black) and

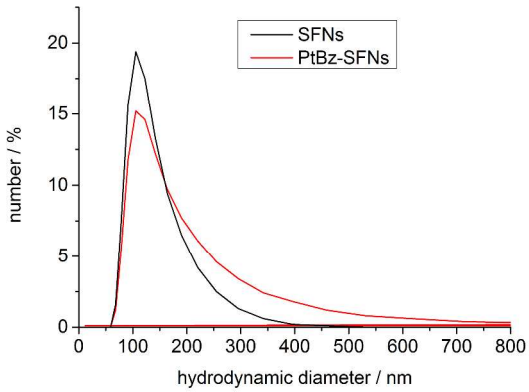

the PtBz-SFNs (red) in 1.5 mL doubly deionized water with the resulting distribution of the hydrodynamic diameter.

Loaded particles were collected by centrifugation. The entrapping of the prodrug was optimized to maximize both loading and efficiency. The Pt content in the PtBz-SFNs was measured from the supernatant by an indirect method by atomic absorption spectrometry (AAS). The determination of the sizes of the NPs was done by dynamic light scattering (DLS). Drug loading in over 15 independent experiments with different batches of nanosilk gave up to 4.1% PtBz loading and maximum drug uptake efficiency of 23%. By using 10 mg/mL (or more) PtBz concentration non-nanometric size particles were obtained. Optimally loaded NPs were generated by using 5 mg/mL of PtBz. These PtBz-SFNs are of adequate size to exploit the EPR effect and they were characterized (Table 1) by DLS, zeta potential measurements, transmission electron microscopy (TEM), scanning electron microscopy (SEM), powder X-ray diffraction (XRD), and IR and Raman spectroscopies.

Table 1 Comparative values for the particle size, polydispersity (PDI), ζ potential and mobility of SFNs and PtBz-SFNs formed by 5 mg/mL drug feed (water at 25 °C).

Sample	Diameter ± Width (nm)	PDI[a]	ζ potential ±SD[b] (mV)	Wall Zeta Potential (mV)	Mobility (µmcm/ Vs)
SFNs	133± 22	0.117 ± 0.01	-20 ± 11	-35.2	-1.6 ± 0.9
PtBz-SFNs	173 ± 57	0.361 ± 0.01	-19 ± 8	-24.4	-1.5 ± 0.6

[a]Average value. [b]Z-average (n = 5) and accumulation times = 100.

For the determination of the SFNs and PtBz-SFNs sizes and size distributions the dry samples were redispersed to a concentration of 1 mg/mL in 1.5 mL doubly deionized water via ultra sonication for 30 min. The dispersions were investigated by

DLS to yield a hydrodynamic diameter for SFNs in the range of 80–400 nm with an average of 133 ± 22 nm (standard deviation σ) (Figure 2). The PtBz-SFNs have a broader diameter distribution of 80–800 nm with an average of 173 ± 57 (Figure 2). The hydrodynamic diameter from DLS is considerably larger than the primary particle size from TEM and SEM measurements (see below). This is apparently due to agglomeration effects.

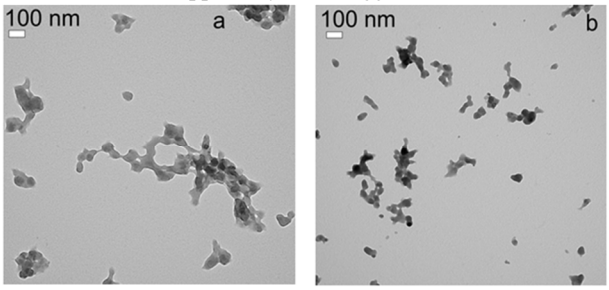

Fig. 3 TEM pictures of SFNs (a) and the PtBz-SFNs (b).

The FT-IR spectra of SFNs and PtBz-SFNs (see Figures S1 and S2) exhibit characteristic absorptions for a water insoluble β-sheet conformation of the silk proteins. Vibrations at 1631cm^{-1} for amide I (C=O stretching), 1528 cm^{-1} for amide II (secondary N–H bending) and 1236 cm^{-1} for amide III (C–N and N–H functionalities) are in agreement with literature data [30]. The small amount of platinum complex compared with silk nanoparticles makes its infrared signals barely perceptible (Figures S1 and S2).

The TEM pictures (Figure 3 and Figure S3) of SFNs and PtBz-SFNs show no obvious differences. No difference in shape or size was monitored in both samples. We think that DLS could differentiate between primary particles and their agglomeration but this may also be due to the redispersion. At higher resolutions primary particles of 50 ± 10 nm size can be observed. A SEM investigation of SFN and PtBz-SFN samples depicted in Figure S4 gave roughly the same results as the TEM pictures. At the highest resolution (Figure S4 bottom row) the primary particle diameter can be determined to about 50 nm which is in agreement with the TEM measurements. Again no difference could be observed in the shape of the nanoparticles for both samples. The macroscopic visual appearance of the samples is slightly different, however. Sample of SFNs looks like gravel and the PtBz-SFN has a fibre morphology when viewed with a naked eye or light microscope (Figure S5). These spherical NPs had an overall moderate negative net charge of –19.1 ± 7.55 mV (very close values to those of SFNs; see Table 1).The surface area of the particles was determined from volumetric nitrogen sorption measurements at 77 K to give a BET surface of 56 m^2/g for SFNs and 60 m^2/g for PtBz-SFNs. Both values are identical within experimental error which is about ± 20 m^2/g. Also a BET surface of about 50 m^2/g corresponds to the outer surface of a fine powder.

Powder X-ray diffraction (PXRD) analysis illustrated that the XRD curves of SFNs and PtBz-SFNs had the characteristic scattering pattern of the β-sheet crystalline silk fibroin (Figure S6). They shows a major peak at 2θ = 20.2º and two shoulders at 9.9º and 24.3º in both loaded and unloaded SFNs. There is no significant difference between the powder patterns of SFNs and the PtBz-SFNs sample.[30] The Raman spectra of SFNs and PtBz-SFNs (Figure S7) showed exactly the same absorptions as reported in the literature for SFNs.[30] The ratio values of the I_{852}/I_{830} (R_{tyr}) bands were 1.29 and 1.45 for lyophilized PtBz-SFNs and unloaded SFNs, respectively (Figure S7). The differences of R_{tyr} values[30,35,48] led to the conclusion that the hydrogen bonds involving the tyrosyl residues in the loaded nanoparticles were weaker than those in the empty SFNs, but stronger than those in lyophilized aqueous silk. In other words, the tyrosine residues around SFNs were more exposed than those around the PtBz-SFNs. UV-spectra of both SFNs and PtBz-SFNs showed a broad absorption in range of 270-285 nm (Figure S8). No significant change in the absorption spectra upon PtBz modification of SFNs was observed.

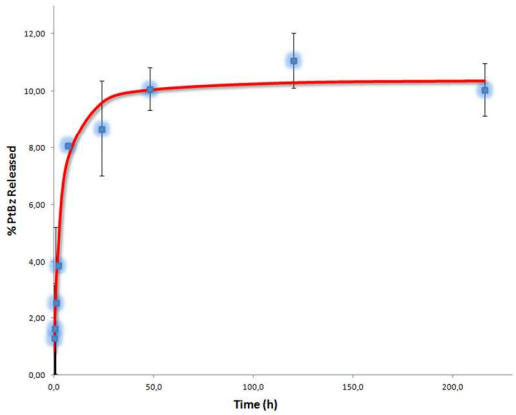

Fig. 4 Release of platinum from PtBz-SFNs in PBS (310 K).

For targeted delivery, drug payload should only be released at the site of its intended target. In order to study the release properties of the NPs, aliquots of PtBz-SFNs suspension were dialyzed against phosphate buffered saline (PBS) at 37 °C over 10 days. The release of platinum, measured by AAS in this and subsequent experiments, during dialysis is presented in Figure 4 as the fraction of entrapped platinum released over time. The results show that only 8.5% of platinum is released during the 48 h keeping the loading constant during the rest of the time. This is in line with the poor water solubility of the drug. In addition, to identify the nature of the release products of PtBz-SFNs, a study by HPLC-MS in water was also undertaken (no PBS used). The unique fraction where platinum peaks were observed showed clusters at 543.00 and 420.97 corresponding to $[PtBz+H]^+$ and the loss of a benzoate group from $PtBz^+$, respectively (Figure S9). Taken together, these findings suggest that most of PtBz could reach the tumor tissue, in spite of its poor aqueous solubility profile.

SFNs cell internalization

As a previous assay to the cytotoxicity study, human endothelial cells EA.hy926 were incubated for 3 h by fluorescein isothiocyanate (FITC) labelled SFNs and then studied by optical microscopy fluorescence. FITC-labelled SFNs are equivalent to non-labelled SFNs in size distribution and cytotoxicity. Cell penetration of labelled nanoparticles can be monitored easily by its intense fluorescence. These images (Figure 5) showed a

significant cell internalization of FITC-SFNs.

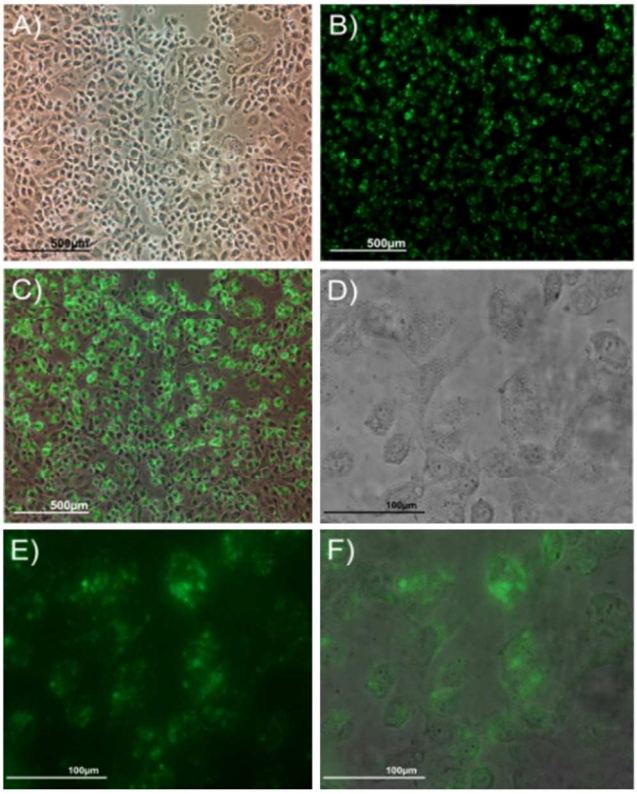

Fig. 5 Different images of the cellular uptake of FITC-labeled silk nanoparticles by endothelial cells (EA.hy926) after incubation for 2 h at 310 K with 7.5% CO_2 atmosphere in a CO_2 incubator. A) Cells under bright field; (B) Cells under fluorescence and (C) Composition of A) and B); D) Cells under phase contrast; E) Cells under fluorescence and F) Composition of D) and E). (Figures A) to C) at 4x magnification, Scale bar = 500 µm; Figures D) to F) at 40x magnification, Scale bar = 100 µm).

Table 2 IC_{50} values [µM] after 72 h of incubation of CDDP, PtBz and PtBz-SFNs prepared by using 5 mg/mL of PtBz expressed as obtained.

Cell Line	CDDP	PtBz	PtBz-SFNs
A2780	2.06 ± 0.30	0.031 ± 0.020	0.09 ± 0.01
A2780cisR	7.60 ± 0.22	0.34 ± 0.00	0.78 ± 0.24
MCF-7	22.70 ± 1.11	0.86 ± 0.04	0.31 ± 0.02
MDA-MB-231	>25	0.59 ± 0.01	0.39 ± 0.15
SK-BR-3	7.20 ± 0.19	0.17 ± 0.01	0.34 ± 0.03
LLC-PK1	4.12 ± 0.13	1.62 ± 0.03	4.20 ± 0.22

PtBz-SFNs antitumor activity

The cytotoxicity of PtBz-SFNs was evaluated (Table 2) toward a panel of human cancer cell lines representative of epithelial ovarian carcinoma cells A2780 and A2780cisR (acquired resistance to cisplatin) and several breast cancer cells: SK-BR-3 (HER2+), MCF-7 (ER+, PR+) and the triple-negative MDA-MB-231 (ER-, PR-, no HER2 overexpression), where cisplatin is not very active. The PtBz-SFNs trigger strong cytotoxic effects, i.e. nanomolar IC_{50} values in all the tumor cell lines essayed, being much more active than cisplatin in all of them: over 20 times in the sensitive to cisplatin A2780 or over 70 times in MCF7. Free platinum SFNs were not cytotoxic in lines A2780 and MCF-7 after 72 h. These results suggest that PtBz-SFNs are able to overcome the resistance mechanisms of ovarian and most breast cancer cells, including the triple negative MDA-MB-231. Furthermore, the cytotoxicity of PtBz-SFNs toward the non-tumorigenic renal cells LCC-PK1 is similar to that of cisplatin and smaller than that of PtBz. The cell selectivity factors (SF = ratio of IC_{50} for LLC-PK1/IC_{50} for A2780 cells) for the PtBz-SFNs (SF = 46.7) are higher than that of CDDP (SF = 2.0).

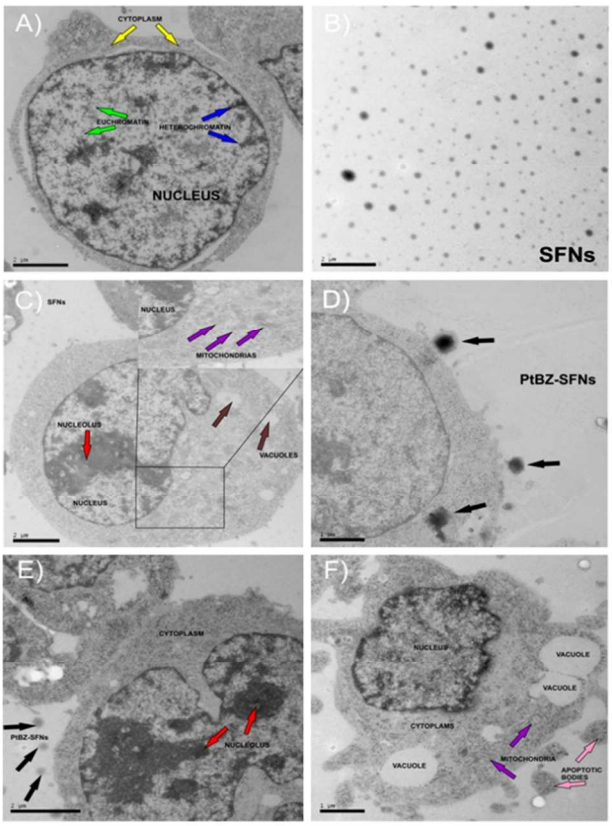

Fig. 6 Images of A2780 cells after 24 h of exposure to: C) and) D) 10 µM of SFNs; E) and F) 10 µM of PtBz-SFNs; In E) early apoptosis is observed; In F) late apoptosis is observed; The inset in (C) shows magnifications. A) control; B) SFNs in the intercellular space.

By using TEM, it seemed likely that we would observe platinum derived contrast in sections of cancer cells treated with the PtBz-SFNs studied here if their deposition is sufficiently localized in cell organelles. A2780 cells were exposed to 1 µM of SFNs or PtBz-SFNs for 24 h, and the treated and control cells

were fixed and embedded in epoxy resin. Ultrathin sections were observed under the TEM (Figure 6). None uranyl acetate nor OsO_4 was used for staining both the control cells and the treated cells. Any additional contrast observed between the control cells and the treated cells is due to cell uptake of SFNs or PtBz-SFNs.

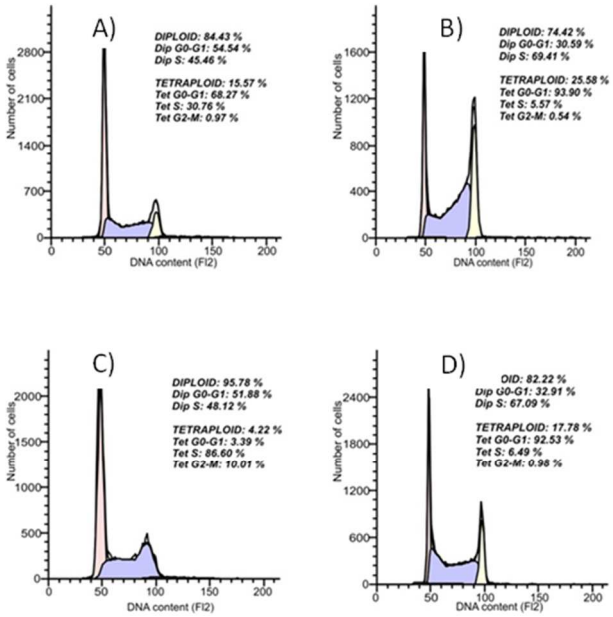

Fig. 7 Cell cycle analysis of A2780 and A2780cisR human ovarian cancer cells after 24 h at 310 K. A) and C) FL2 histograms for negative controls: cells untreated (A2780 and A2780cisR, respectively); B) and D) FL2 histograms for cells exposed to PtBz-SFNs, concentration used was 0.5 μM.

Sections of cells treated with 1 μM of PtBz-SFNs show more contrast in comparison to those from control cells in the nucleolus and the internal nuclear membrane (Figure 6E). Several cells displayed the morphological changes associated with apoptosis (Figures 6E and 6F).

To understand the effect of PtBz-NFSs on cell growth we examined their effect on the cell cycle by FACS (Fluorescence Activated Cell Sorter) analysis. Treatment of A2780 and A2780cisR cell lines with 0.5 μM of PtBz-SFNs (approximately the IC_{50} value for the NPs in respect to A2780 cells) for 24 h (Figure 7) showed a significant increase of these cells in the S and G2 phases, with a corresponding reduction of those in G0/G1, as observed also in cisplatin. The emergence of a tetraploid cell population unable to divide occurred (Figure 7B). Cell cycle analysis of MCF-7, MDA-MB-231 and SK-BR-3 cancer cells was also undertaken (Figure S10). Apoptotic studies were also carried out with all cell lines. Exposure of phosphatidylserine (PS) was followed by a flow cytometric assay with the Annexin V-FLUOS apoptosis detection kit (Roche). Propidium iodide (PI) was also applied to stain necrotic or late apoptotic cells. Fluorescence intensity was measured for each cell by flux cytometry. The results for MDA-MB-231 cells are shown in Figure 8. The four typical quadrants identifying the living (lower left quadrant D1, not or low stained cells), the early apoptotic (lower right quadrant D2, only the annexin-V stained cells), the necrotic (upper-left quadrant D4, only PI stained cells) and the late apoptotic (upper right quadrant D3, cells stained with both fluorescent dyes) cells appear in these diagrams. As it can be seen clearly PtBz-SFNs induce a high incidence of late stage apoptosis in MDA–MB–231 cells. Similar results were observed in the rest of cells assayed (Supporting Information, Figures S11 and S12).

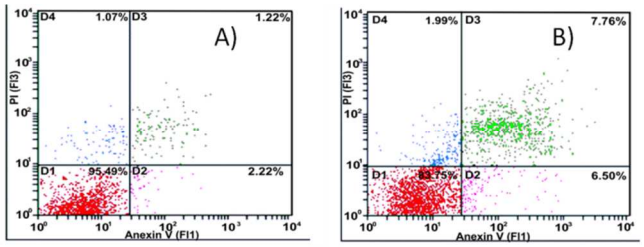

Fig. 8 Flow cytometry analysis of MDA-MB-231 human breast cancer cells after treatment with PtBz-SFNs as detected by annexin V/PI. Density plots for A) untreated cells (control) and for B) cells treated with 1 μM (24 h) PtBz-SFNs. The experiments were performed in triplicate.

4. Conclusions

In summary, we have successfully generated SNFs loaded with a hydrophobic platinum(IV) produg, PtBz. Only a small fraction of the loaded PtBz is released (less than 10% after 48 h). PtBz-SFNs are very cytotoxic (nanomolar IC_{50} values) toward the ovarian cell line A2780 and A2780cisR, and several breast tumor cell lines SK-BR-3, MCF-7 and MDA-MB-231, overcoming drug resistance to cisplatin. Interestingly, the PtBz-SFNs are poor active against the non-tumorogenic renal cells LLC-PK1. The cell selectivity factors (SF = ratio of IC_{50} for LLC-PK1/IC_{50} for A2780 cells) for the PtBz-SFNs (SF = 46.7) are higher than that of **C**DDP (SF = 2.0). Therefore, loading on SFNs can ameliorate the delivery of the poorly soluble PtBz and reduce its toxicity towards non-tumorigenic cells. TEM images showed high electron density in the nucleus of A2780 cells. PtBz-SFNs cause cell cycle arrest in the S and G2 phases and induce late stage apoptosis.

Acknowledgments

This work was supported by the Spanish Ministerio de Economía y Competitividad and FEDER/ERDF (Project SAF2011-26611) and by Fundación Séneca-CARM (Project 15354/PI/10). COST CM1105 for providing opportunities of discussion, and Dr. Ignacio López for AAS assistance are also acknowledged. Dr. A. Abel Lozano-Pérez's research contract was partially supported (80%) by the FEDER/ERDF of the Region of Murcia 2007–2013.

Notes and references

[a] *Instituto Murciano de Investigación y Desarrollo Agrario y Alimentario (IMIDA), E-30150 La Alberca, Murcia, Spain.*
[b] *Departamento de Química Inorgánica, Universidad de Murcia and Instituto Murciano de Investigación Biosanitaria IMIB-Arrixaca, E-30071 Murcia, Spain.. Fax: +34 868 88 41 48; Tel: +34 868 88 74 55; E-mail: jruiz@um.es*
[c] *Institut für Anorganische Chemie und Strukturchemie, Universität Düsseldorf, D-40204 Düsseldorf, Germany.*

† Electronic Supplementary Information (ESI) available: [Additional figures regarding characterization of NPs and biological study details supplied]. See DOI: 10.1039/b000000x/

1 M. A. Fuertes, C. Alonso and J. M. Pérez, *Chem. Rev.*, 2003, **103**, 645–662.
2 D. Wang and S. J. Lippard, *Nat. Rev. Drug Discov.*, 2005, 4, 307–320.
3 Y. Min, C.-Q. Mao, S. Chen, G. Ma, J. Wang and Y. Liu, *Angew. Chem. Int. Ed.*, 2012, **51**, 6742–6747.
4 L. R. Kelland, *Nat. Rev. Cancer*, 2007, *7*, 573–584; b) L. R. Kelland, *Drugs*, 2000, **59**, 1–8.
5 M. D. Hall, H. R. Mellor, R. Callaghan and T. W. Hambley, *J. Med. Chem.*, 2007, **50**, 3403–3411.
6 N. Graf, S. J. Lippard, *Adv. Drug Deliv. Rev*. 2012, **64**, 993–1004.
7 R. K. Jain and T. Stylianopoulos, *Nat. Rev. Clin. Oncol.*, 2010, **7**, 653–664.
8 C. R. Maldonado, L. Salassa, N. Gómez-Blanco and J. C. Mareque-Rivas, *Coord. Chem. Rev.*, 2013, **257**, 2668–2688.
9 D. Peer, J. M. Karp, S. Hong, O. C. FaroKHzad, R. Margalit and R. Langer, *Nat. Nanotechnol.*, 2007, **2**, 751–760.
10 H. Cabral, N. Nishiyama and K. Kataoka, *Acc. Chem. Res.*, 2011, **44**, 999–1008.
11 A. Ozgur, F. Y. Lambrecht, K. Ocakoglu, C. Gunduz and M. Yucebas, *Int. J. Pharm.*, 2012, **422**, 472–478.
12 N. Kamaly, Z. Xiao, P. M. Valencia, A. F. Radovic-Moreno and O. C. Farokhzad, *Chem. Soc. Rev.*, 2012, **41**, 2971–3010.
13 J. Della Rocca and D. Liu, W. Lin, *Acc. Chem. Res.*, 2011, **44**, 957–968.
14 U. Prabhakar, H. Maeda, R. K. Jain, E. M. Sevick-Muraca, W. Zamboni, O. C. Farokhzad, S. T. Barry, A. Gabizon, P. Grodzinski and D. C. Blakey, *Cancer Res*., 2013, **73**, 2417–2417.
15 W. H. Ang, I. Khalaila, C. S. Allardyce, L. Juillerat-Jeanneret, P. J. Dyson, *J. Am. Chem. Soc.*, 2005, **127**, 1382–1383.
16 S. Dhar and S. J. Lippard, *Proc. Natl. Acad. Sci. U.S.A.*, 2009, 106, 22199–22204.
17 S. Dhar, F. X. Gu, R. Langer, O. C. Farokhzad and S. J. Lippard, *Proc. Natl. Acad. Sci. U.S.A.*, 2008, **105**, 17356–17361.
18 N. Kolishetti, S. Dhar, P. M. Valencia, L. Q. Lin, R. Karnik, S. J. Lippard, R. Langer and O. C Farokhzad, *Proc. Natl. Acad. Sci. U.S.A.*, 2010, **107**, 17939–17944.
19 S. Dhar, N. Kolishetti, S. J. Lippard and O. C Farokhzad, *Proc. Natl. Acad. Sci. U.S.A.*, 2011, **108**, 1850–1855.
20 N. Graf, D. R. Bielenberg, N. Kolishetti, C. Muus, J. Banyard, O. C Farokhzad and S. J. Lippard, *ACS Nano*, 2012, **6**, 4530–4539.
21 D. Moreno, S. Zalba, I. Navarro, C.T. de Ilarduya and M.J. Garrido, *Eur. J. Pharm. Biopharm.*, 2010, **74**, 265–274.
22 Y. Min, J. Li, F. Liu, E. K. L. Yeow and B. Xing, *Angew. Chem. Int. Ed.*, 2014, 53, 1012–1016.
23 Y. Min, C.-Q. Mao, S. Chen, G. Ma, J. Wang and Y. Liu, *Angew. Chem. Int. Ed.*, 2012, **51**, 6742–6747.
24 T. Kean and M. Thanou, *Adv. Drug Deliv. Rev.*, 2010, **62**, 3–11.
25 H. S. Oberoi, N. V. Nukolova, A. V. Kabanov and T. K. Bronich, *Adv. Drug Deliv. Rev.*, 2013, **65**, 1667–1685.
26 J. Li, S. Q. Yap, C. F. Chin, Q. Tian, S. L. Yoong, G. Pastorin and W. H. Ang, *Chem. Sci*., 2012, **3**, 2083–2087.
27 C. Vepari, D. L. Kaplan, *Prog. Polym. Sci.*, 2007, **32**, 991–1007.
28 Q. Lu, X. Wang, H. Zhu and D. L. Kaplan, *Acta Biomater.*, 2011, **7**, 2782–2786.
29 M. Chen, Z. Shao and X. Chen, *J. Biomed. Mater. Res. A*., 2012, **100**, 203–210.
30 Y. Q. Zhang, W. D. Shen, R. L. Xiang, L. J. Zhuge, W. J. Gao and W.B. Wang, *J. Nanoparticle Res.*, 2007, **9**, 885–900.
31 A. B. Mathur and V. Gupta, *Nanomedicine*, 2010, *5*, 807–820.
32 Y.-R. Zheng, K. Suntharalingam, T. C. Johnstone, H. Yoo, W. Lin, J. G. Brooks and S. J. Lippard, *J. Am. Chem. Soc.*, 2014, **136**, 8790–8798.
33 F. G. Omenetto, D. L. Kaplan, *Science*, 2010, **329**, 528–531.
34 B. Subia and S. C. Kundu, *Nanotechnology*, 2013, **24**, 035103.
35 E. M. Pritchard and D. L. Kaplan, *Expert Opin. Drug. Deliv.*, 2011, **8**, 797–811.
36 B. Subia, S. Chandra, S. Talukdara and S. C. Kundu, *Integr. Biol.*, 2014, **6**, 203–214.
37 A. Matsumoto, J. Chen, A. L. Collette, U. J. Kim, G. H. Altman, P. Cebe and D. L. Kaplan, *J. Phys. Chem.*, 2006, **110**, 21630–21638.
38 B. Kundu, N. E. Kurland, S. Banoa, C. Patrac, F. B. Engel, V. K. Yadavalli and S. C. Kundu, *Prog. Polymer Science*, 2014, **39**, 251–267.
39 P. G. Shi, T. S. K. Teh, S. L. Toh and J. C. H. Goh, *Biomaterials*, 2013, **34**, 5947–5957.
40 W. Zhang, J. L. Chen, J. D. Tao, C. C. Hu, L. K. Chen, H.S. Zhao, G. W. Xu, B. C. Heng and H. W. Ouyang, *Biomaterials*, 2013, **34**, 6046–6057.
41 Y. Gu, J. B. Zhu, C. B. Xue, Z. M. Y. Li, F. Ding, Y. M. Yang and X. S. Gu, *Biomaterials*, 2014, **35**, 2253–2263.
42 N. Kasoju and U. Bora, *Adv. Health. Mater.*, 2012, **1**, 393–412.
43 C. Y. Wang, K. H. Zhang, C. Y. Fan, X. M. Mo, H. J. Ruan and F. F. Li, *Acta Biomater.*, 2011, **7**, 634-643.
44 F. P. Seib, G. T. Jones, J. Rnjak-Kovacina, Y. Lin and D. L. Kaplan, *Adv. Health. Mater.*, 2013, **2**, 1606–1611**.**
45 J. Qu, Y. Liu, Y. Yu, J.Li, J. Luo and M. Li, *Mater. Sci. Eng. C*, 2014, **44**, 166–174.
46 R. J. Brandon and J. C. Dabrowiak, *J. Med. Chem.*, **1984**, *27*, 861–865.
47 T. R. Chen, *Tca Manual*, 1975, **1**, 229–232.
48 Siamwiza, R. C. Lord, M. C. Chen, T. Takamatsu, I. Harada, H. Matsuura and T. Shimanouchi, *Biochemistry*, 1975, **14**, 4870–4876.

Graphical Abstract

We have successfully generated silk nanoparticles loaded with the hydrophobic platinum(IV) antitumor produg PtBz achieving high cell selectivity factors.